Spectroscopic characterization of Mn^{2+} and Cd^{2+} coordination to phosphorothioates in the conserved A9 metal site of the hammerhead ribozyme

Laura M. Hunsicker-Wang,[a] Matthew J. Vogt,[b] Charles G. Hoogstraten,[c] Nathaniel J. Cosper,[d] Audrey M. Davenport,[e,f] Christopher H. Hendon,[e,f] Robert A. Scott,[g] R. David Britt,[h] Victoria J. DeRose[e,f,*]

(a) Current address: Department of Chemistry, Trinity University, San Antonio, TX

(b) Current address: Office of Extramural Research Policy and Operations, National Institute of Allergy and Infectious Diseases, Bethesda, MD

(c) Current address: Department of Biochemistry, Michigan State University, East Lansing MI

(d) Current address: Brady-Built, Inc., Auburn MA

(e) Department of Chemistry and Biochemistry, University of Oregon, Eugene, OR

(f) Materials Science Institute, University of Oregon, Eugene, OR

(g) Department of Chemistry and Center for Metalloenzyme Studies, University of Georgia, Athens, GA

(h) Department of Chemistry, University of California-Davis, Davis, CA

*Corresponding author. derose@uoregon.edu

Abstract

Phosphorothioate modifications have widespread use in the field of nucleic acids. As substitution of sulfur for oxygen can alter metal coordination preferences, the phosphorothioate metal-rescue experiment is a powerful method for identifying metal coordination sites that influence specific properties in a large RNAs. The A9/G10.1 metal binding site of the hammerhead ribozyme (HHRz) has previously been shown to be functionally important through phosphorothioate rescue experiments. While an A9-S$_{R\mathrm{p}}$ substitution is inhibitory in Mg^{2+}, thiophilic Cd^{2+} rescues HHRz activity. Mn^{2+} is also often used in phosphorothioate metal-rescue studies but does not support activity for the A9-S$_{R\mathrm{p}}$ HHRz. Here, we use EPR, electron spin-echo envelope modulation (ESEEM), and X-ray absorption spectroscopic methods to directly probe the structural consequences of Mn^{2+} and Cd^{2+} coordination to R_p and S_p phosphorothioate modifications at the A9/G10.1 site in the truncated hammerhead ribozyme (tHHRz). The results demonstrate that while Cd^{2+} does indeed bind to S in the thio-substituted ligand, Mn^{2+} coordinates to the non-sulfur oxo group of this phosphorothioate, regardless of isomer. Computational models demonstrate the energetic preference of Mn-O over Mn-S coordination in metal-dimethylthiophosphate models. In the case of the tHHRz, the resulting Mn^{2+} coordination preference of oxygen in either R_p or S_p A9 phosphorothioates differentially tunes catalytic activity, with Mn-O coordination in the A9-S$_{R\mathrm{p}}$ phosphorothioate enzyme being inhibitory.

Keywords

Phosphorothioate, metals, spectroscopy, ribozyme, RNA, EPR, ESEEM, EXAFS, hammerhead, computation, DFT

Introduction

Establishing the influence of specific metal sites on RNA function is challenging due to the polyanionic nature of the biopolymer and large number of nonspecific cation interactions [1,2,3]. The phosphorothioate metal-rescue experiment (PS-rescue) is a powerful method for identifying metal coordination sites that influence specific properties in a large RNAs. In a PS-rescue experiment, a single phosphate oxygen is changed to sulfur and subsequent changes in metal ion specificity are monitored, testing the hypothesis that a metal ion binds directly to that particular phosphate oxygen [1,4,5]. A premise of PS-rescue experiments is that sulfur substitutions of phosphate oxygens to create phosphorothiolate (bridging oxygen) and phosphorothioates (non-bridging oxygen, Fig. 1A) are proposed to decrease the affinity of hard metals such as Mg^{2+} for the substituted group, resulting in decreased activity of the ribozyme if that metal-oxygen interaction is important for ribozyme function. If the addition of a thiophilic metal such as Cd^{2+} rescues catalysis, there is strong evidence for inner-sphere metal ion coordination at that site. Phosphorothioate substitutions are stereospecific, resulting in R_p- and S_p- isomers that further pinpoint the identity of the potential metal ligand.

Phosphorothioates are also important in oligonucleotide therapeutics, where they provide protection from cellular nucleases as well as influence cellular uptake [6]. Few studies have reported the structural consequences of PS-substitution [7-11] or the structural impacts on metal coordination [12-14]. In ribozyme PS-rescue studies, Mn^{2+} is sometimes used as the 'thiophilic' rescue metal. Although Mn is more thiophilic than Mg^{2+}, the selectivity of Mn^{2+} for a thiolate ligand in the midst of oxo-donor options is not clear [14], in particular in the context of complex RNA structures.

Here, we use spectroscopic methods to directly probe the structural consequences of Mn^{2+} and Cd^{2+} coordination to R_p and S_p phosphorothioate modifications at a known metal site in the truncated hammerhead ribozyme (tHHRz). The results demonstrate that while Cd^{2+} does bind to sulfur in the thio-substituted ligand, Mn^{2+} coordinates to the non-sulfur oxo group of this phosphorothioate, regardless of isomer. The resulting Mn^{2+} coordination preference dramatically tunes catalytic activity in the tHHRz.

The Hammerhead ribozyme (HHRz) is one of the earliest-discovered ribozymes and has been the subject of many mechanistic studies aimed at understanding RNA-directed catalysis at the molecular level [17,18]. This self-cleaving RNA motif (Fig. 1a) was originally discovered in

plant viroids, where it functions in genomic processing during rolling circle replication [19,20].

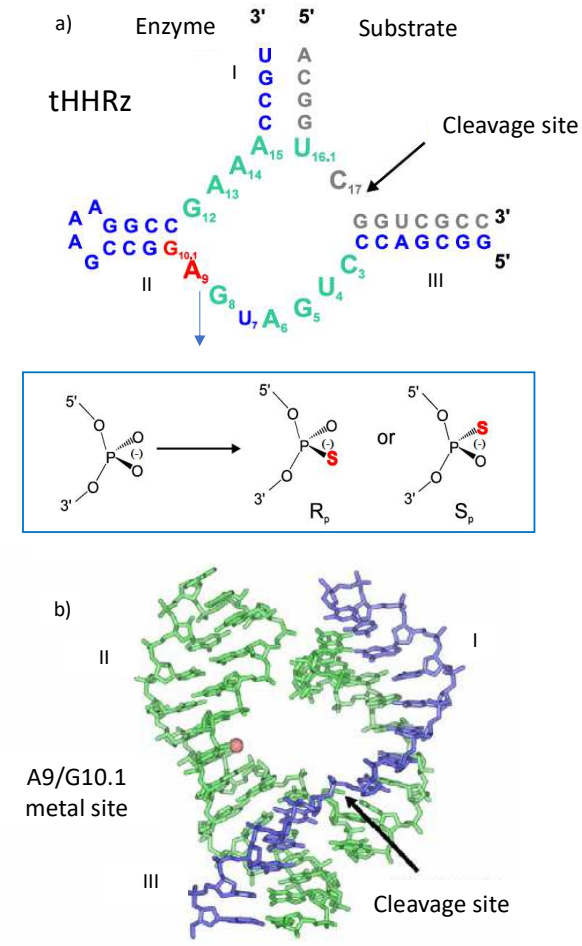

Figure 1. Truncated hammerhead ribozyme (tHHRz) used in these studies. a) Secondary structure representation with the enzyme strand in blue, the substrate strand in gray, the conserved core nucleotides in aqua, and A9 and G10.1 shown in red. Cleavage site denoted by arrow at right. Inset shows a phosphorothioate, with substitution of a non-bridging phosphodiester oxygen with a sulfur and R_p or S_p isomers. b) The tHHRz crystal structure PDB 1HMH with substrate strand in blue and enzyme strand in green. The sphere represents a metal ion at the A9/G10.1 site.

The HHRz motif has since been discovered in other genomes including a discontinuous motif in mouse [21]. The function of the HHRz in higher organisms is unknown. The HHRz active site is created by a conserved core of nucleotides that is surrounded by three helices and has been studied in vitro as a truncated (tHHRz) as well as in an extended form, the latter of which preserves important tertiary interactions between helical stems I and II.

The HHRz catalyzes attack of a 2′-OH on its proximal 3′-phosphodiester bond, resulting in a cyclic phosphate and 5′-OH products. As with most ribozymes, the *in vitro* reaction is

sensitive to ionic conditions and at moderate ionic strength the HHRz reaction is enhanced by the presence of divalent cations [1,18,22,23]. Several lines of evidence demonstrate that a metal ion bound at the 'A9/G10.1 site' modulates hammerhead ribozyme activity [24,25,26,27,28,29]. Across numerous PS-inhibition studies, only thiophosphates placed 5′ to A9 and to the cleavage site were shown to inhibit activity in Mg^{2+} *and* have their effects be rescued by thiophilic Cd^{2+}. These results suggested both the A9 and cleavage site as potential metal ligands important to hammerhead activity [24,25]. For the tHHRz, substitution of the A9 phosphate with an R_p-phosphorothioate (A9-S_{Rp}) results in at least a 500-fold reduction in the rate of catalysis in the presence of Mg^{2+} whereas Mg^{2+} -dependent activity for the S_p isomer (A9-S_{Sp}) is relatively unaffected. Addition of Cd^{2+}, in a background of Mg^{2+} or Ca^{2+}, rescues A9-S_{Rp} catalytic activity, supporting the idea that the modified phosphate is part of a functional metal site [24,25].

The exact role of the A9/G10.1 metal site in HHRz catalysis is unresolved. Critical roles for nucleobases in the HHRz reaction, and potential roles for metals to influence nucleobase pK_a, have been discussed [28-32]. Original X-ray crystallographic structures of the tHHRz (Figure 1b) exhibit an 'open' conformation wherein the A9/G10.1 metal site is distant from the cleavage site [26,27]. Nonetheless, based on early double-phosphorothioate substitution studies on the tHHRz, a model was proposed in which the metal bound at the A9 site also adopts the cleavage site scissile phosphate as a ligand in the activated form of the ribozyme [24]. Subsequent structures of extended HHRz constructs that maintain tertiary interactions between Stems I and II show a closer proximity of the A9/G10.1 site to the cleavage site [29, 32], and the distance is further reduced in the structure of a vanadate-substituted transition state analogue [30]. Mechanistic modeling suggests a model in which the A9/G10.1 metal ion may undergo ligand exchange to activate the cleavage site phosphodiester bond [31]. In the extended HHRz construct, both the A9 and cleavage site are still sensitive to phosphorothioate substitution [22], and thermodynamic analysis of Cd^{2+} rescue of the scissile phosphorothioate supports a ground-state metal interaction [33]. While the exact role of the A9/G10.1 metal site in the mechanism of the HHRz is not completely resolved, this metal site is functionally important.

We have previously pursued direct detection of metal ions in the hammerhead ribozyme by magnetic resonance spectroscopic methods, including EPR spectroscopy with paramagnetic Mn^{2+} [34-36] and ^{31}P NMR in conjunction with phosphorothioate substitutions [14]. In the tHHRz a high-affinity metal site can be uniquely populated by Mn^{2+} with an apparent $K_d \leq 10$

μM even in a background of 1 M competing monovalent Na^+ ions. Mn^{2+} occupying this site has a characteristic EPR lineshape feature [34,35]. Hyperfine couplings between the Mn^{2+} and ligand ^{31}P and ^{1}H nuclei were observed by electron-nuclear double resonance (ENDOR) spectroscopy [35]. Electron spin echo envelope modulation (ESEEM) spectroscopic measurements identified $^{14}N/^{15}N$ couplings [36,37] ascribed to the G10.1 nucleobase through site-specific ^{15}N labeling [38]. These measurements assign this high-affinity Mn^{2+} to the A9/G10.1 site, consisting of a Mn^{2+} chelated by A9 phosphodiester and G10.1 imino N ligands, with four aqua ligands. With these spectroscopic signals, we can follow the molecular details of metal coordination at this important ribozyme cation site.

Here we employ spectroscopic methods to determine the effect of a phosphorothioate substitution 5′ to A9 (A9-S_{Rp} or A9-S_{Sp}) on the specific coordination environment of Mn^{2+} in the tHHRz A9/G10.1 site. We use EPR, ESEEM, and Extended X-Ray Absorption Fine Structure (EXAFS) spectroscopies to determine the Mn^{2+} coordination environment with either an R_p or S_p thiophosphate at A9. Although it is more thiophilic than Mg^{2+}, Mn^{2+} does not rescue activity in the A9-S_{Rp} hammerhead ribozyme. We are able to show that Mn^{2+} binds to this site, but does not coordinate the sulfur ligand in the A9-S_{Rp} isomer. By contrast, Cd^{2+} does bind to sulfur in this isomer and supports activity. These data suggest a new basis for inhibition by thiophosphate substitutions in which a metal ion may ligate to the alternate oxygen ligand of the phosphorothioate, forcing a structure that does not support activity. The results demonstrate that a simple switch of metal ion ligands can govern RNA catalysis, and reinforce the importance of using the more thiophilic Cd^{2+} for ribozyme phosphorothioate interference studies.

Results

The basis of a phosphorothioate (PS)-rescue experiment is that the sulfur substituted into the non-bridging oxygen position is a poor ligand for a functionally-important Mg^{2+}, but that coordination of a more thiophilic metal ion can rescue activity. Both Mn^{2+} and Cd^{2+} are commonly utilized for PS-rescue, based on their higher thiophilicity compared to Mg^{2+}. For the hammerhead A9 site, PS-rescue with Cd^{2+} has been reported [24,25]. We first ascertained the ability of Mn^{2+} to support activity with a phosphorothioate substitution at the A9 position of the tHHRz. Activity studies were performed in a background of 1 M NaCl, which has previously been used for spectroscopic experiments [34-36,38]. Substitution of the phosphate 5′ to A9 with

an Rp phosphorothioate (A9-S$_{Rp}$) has a dramatic negative effect on Mn^{2+}- dependent cleavage activity (Figure 2a), as has previously been observed in the presence of Mg^{2+} [24,25]. Monitored at 5 mM Mn^{2+}, the R_p substitution (A9-S$_{Rp}$) has eliminated activity, whereas the S_p isomer maintains wild-type rates (inset, Figure 2a). Cd^{2+} rescues activity in the A9-S$_{Rp}$ hammerhead (Figure 2b) at concentrations in which Mn^{2+} does not support detectable cleavage. These Cd^{2+} rescue data are consistent with a simple interpretation that metal ions bind to the pro-R_p position of the tHHRz A9 5′ phosphodiester. The activity studies also demonstrate that Mn^{2+} is not able to effectively rescue the A9-S$_{Rp}$ substitution in the tHHRz. This could be due to a loss of Mn coordination at this site, or a change in ligands. To understand the influence of metal coordination at the A9 metal site on activity, we employed spectroscopic techniques to examine metal coordination at this site in the tHHRz.

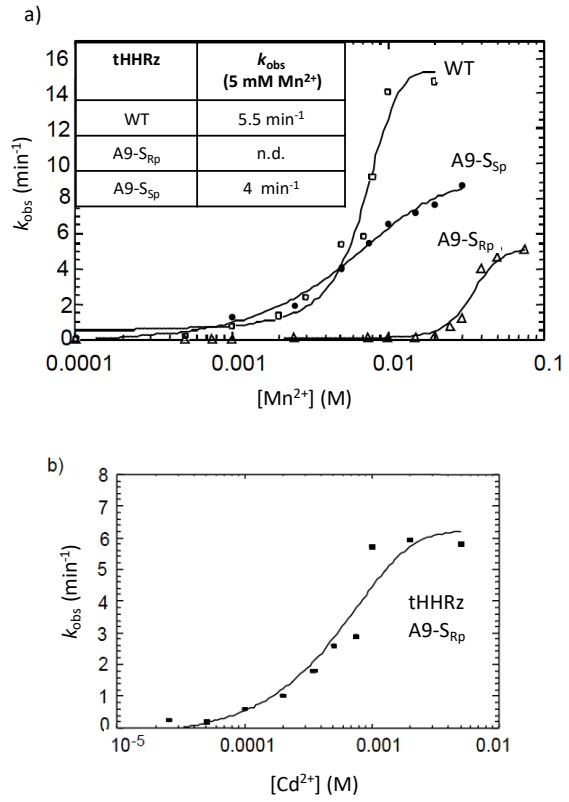

Figure 2. Activity of the wild type and A9-phosphorothioate substituted tHHRz. a) Single-turnover rate profile of WT, A9-S$_{Sp}$ and A9-S$_{Rp}$ with added Mn^{2+} in a background of 1 M Na^+, pH 7.0. Inset shows rate constants at 5 mM Mn^{2+}. b) Single-turnover rate profile of A9-S$_{Rp}$ with added Cd^{2+} in a background of 10 mM Mn^{2+}, 1 M Na^+, pH 7.0. Line is drawn for presentation.

Low temperature Mn^{2+} EPR spectroscopy

EPR spectroscopy was used to address the initial question of whether Mn^{2+} is able to occupy the A9/G10.1 site with a phosphorothioate 5′ to A9. For Mn^{2+} bound in the high affinity site of the unaltered tHHRz, the low temperature EPR spectrum has a subtle but reproducible spectral signature that is most obvious as a change in the sixth line of the derivative lineshape (Figure 3a) [35,39,40]. Mn^{2+} EPR spectra at this frequency are dominated by the $M_S=\pm 1/2$ manifold of the S=5/2 spin system interacting with the I=5/2 ^{55}Mn nuclear spin, giving rise to six central transitions. The sixth-line feature highlighted in Figure 3 reflects additional structure due to 'forbidden' $\Delta M_S=1$, $\Delta M_I=1$ transitions that arise in the presence of zero-field splitting. A multifrequency EPR analysis of this lineshape change in comparison with Mn-nucleotide models [40] resulted in the conclusion that the sharpening of this feature in the Mn-HHRz sample is not due to significant changes in zero-field splitting parameters, but instead is due to decreased linebroadening, suggesting that the Mn^{2+}-ribozyme environment is more homogeneous than that of model systems. A more homogeneous metal-ligand environment may be due to exclusion of solvent and ordering of bound aqua ligands in the ribozyme environment. At a 1:1 ratio of Mn:RNA, this lineshape change is only observed in the hammerhead samples and is not observed for Mn^{2+} in buffer, duplex RNA, or a mutant ribozyme in which all conserved core nucleotides are replaced by U [35,39].

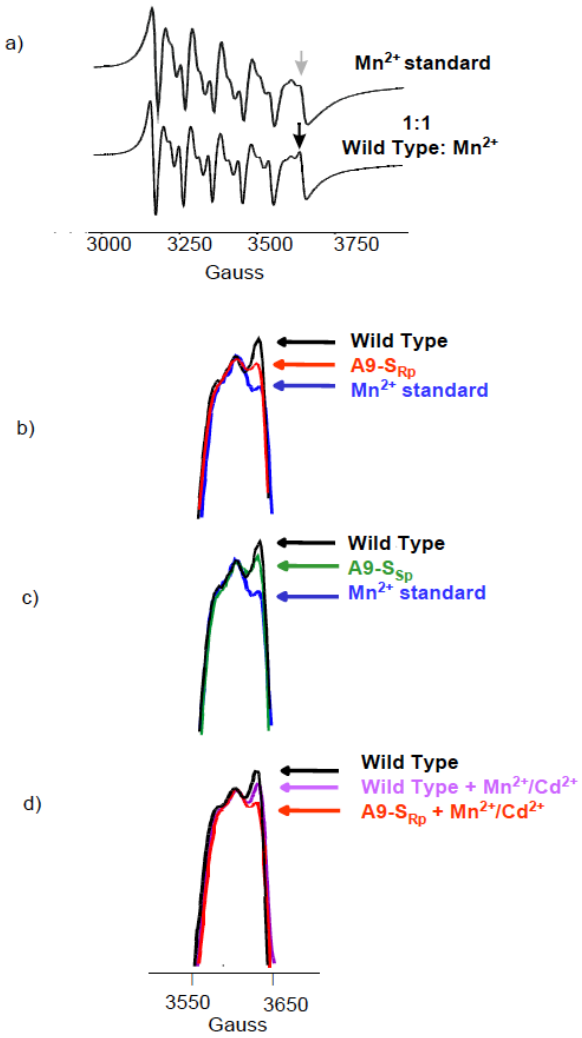

Figure 3. Low temperature Mn^{2+} EPR spectra of wild type, A9-S_{Sp}, and A9-S_{Rp} tHHRz with 1 equivalent of Mn^{2+}. a) Full, low temperature EPR spectra of Mn^{2+} in buffer and wild type ribozyme in a ratio of 1:1 Mn:HHRz. Black arrows denote spectroscopic signature feature, gray arrows denote lack of feature. Enlarged comparison of sixth line in b) wild type (black), A9-S_{Rp} (red), and buffer (blue) c) wild type (black), A9-S_{Sp} (green), and buffer (blue) and d) wild type (black), 1:1:1 Mn:Cd:wild type (purple), and 1:1:1 Mn:Cd: A9-S_{Rp} (red). All samples in 5 mM TEA, pH 7.8 1 M Na^+, 20% v/v ethylene glycol, 10 K, 0.063 mW.

The low temperature Mn^{2+} EPR spectra of A9-S_{Sp} and A9-S_{Rp} compared to wild type tHHRz and Mn^{2+} in buffer are shown in Figure 3a, b, and c. The distinctive Mn^{2+} EPR spectral feature is still observed in both A9-S samples, although it is diminished in intensity in A9-S_{Rp} in comparison to wild type (Figure 3b). This Mn^{2+} EPR feature is present in wild type tHHRz samples for which ENDOR and ESEEM experiments [35,36] have shown phosphate and nitrogen coordination respectively, and its observation in the A9-S_{Rp} and A9-S_{Sp} samples is

consistent with Mn^{2+} populating the tHHRz A9 site in the presence of phosphorothioate substitutions.

It might be expected that the more thiophilic Cd^{2+} would have a greater affinity than Mn^{2+} for the A9-S site. Displacing Mn^{2+} by Cd^{2+} would result in a Mn^{2+} EPR signal characteristic of the unbound ion and lacking the distinctive lineshape feature. Addition of 1 equivalent of Cd^{2+} to the A9-S_{Rp} hammerhead indeed effects a complete loss of the hammerhead-related Mn^{2+} EPR signature (Figure 3d), consistent with Cd^{2+} replacing the Mn^{2+} ion at this phosphorothioate-substituted site. When the same experiment is performed using the wild type hammerhead lacking the sulfur substitution at A9, the Mn^{2+} EPR signal remains unaffected by addition of Cd^{2+} (Figure 3d). These competition experiments suggest that in the absence of sulfur substitution at the A9 pro-R_p site, Mn^{2+} has a higher affinity for this site than does Cd^{2+}.

ESEEM spectroscopy: Mn^{2+} coordinates nucleobase ligands in A9-S_{Sp} and A9-S_{Rp} tHHRz samples

If Mn^{2+} binds to the A9/G10.1 site even upon A9 phosphorothioate substitution, Mn^{2+} coordination to the N7 position of G10.1 should also be observed. ESEEM (Electron Spin Echo Envelope Modulation) spectroscopy is particularly sensitive for detecting weakly coupled, quadrupolar nuclei such as previously observed for Mn^{2+}-N7 guanine (or adenine) interactions [36-38,41]. ESEEM spectroscopy was therefore used to detect nitrogen coordination to Mn^{2+} in the A9-S_{Sp} and A9-S_{Rp} phosphorothioate-substituted tHHRz. The Fourier transformed (FT) data for 2-pulse and 3-pulse ESEEM collected on tHHRz A9-S_{Sp} and A9-S_{Rp} samples are shown in Figure 4a, in comparison with data for Mn^{2+} in the wild type tHHRz run under the same conditions. The 2-pulse FT spectra of all three samples show four low frequency features at around 0.6, 1.9, 2.8, and 5.2 MHz. As previously determined for WT tHHRz, these features are attributable to modulation from guanine ^{14}N interactions [36] that were assigned to G10.1 through ^{15}N labeling [36,38], and were previously modeled with hyperfine (A_{iso}~2.3 MHz) and nuclear quadrupole (e^2qQ~3 MHz, η~0.4) parameters similar to those observed for Mn-guanine model systems [41]. The similarity of ESEEM spectra in Figure 4 indicates that Mn^{2+} coordination to nitrogen in the tHHRz is largely unchanged upon phosphorothioate substitution. The A9-S_{Rp} sample exhibits slightly lower modulation depth of the time-domain spin echo modulation that is likely due to a decreased metal ion population at that site compared to the wild

type or A9-S_{Sp} hammerheads (Figure S1). Three-pulse data for Mn^{2+} bound to the A9-S_{Sp} and A9-S_{Rp} samples similarly show ESEEM features previously attributed to Mn-guanine in the tHHRz and that are not observed in Mn^{2+} - buffer control samples (Figure 4b). The 3-pulse ESEEM data show an additional small peak at ~4 MHz that is assigned as ^{23}Na from weakly coupled Na^+ ions present in the 1 M Na^+ buffer [37,41,42].

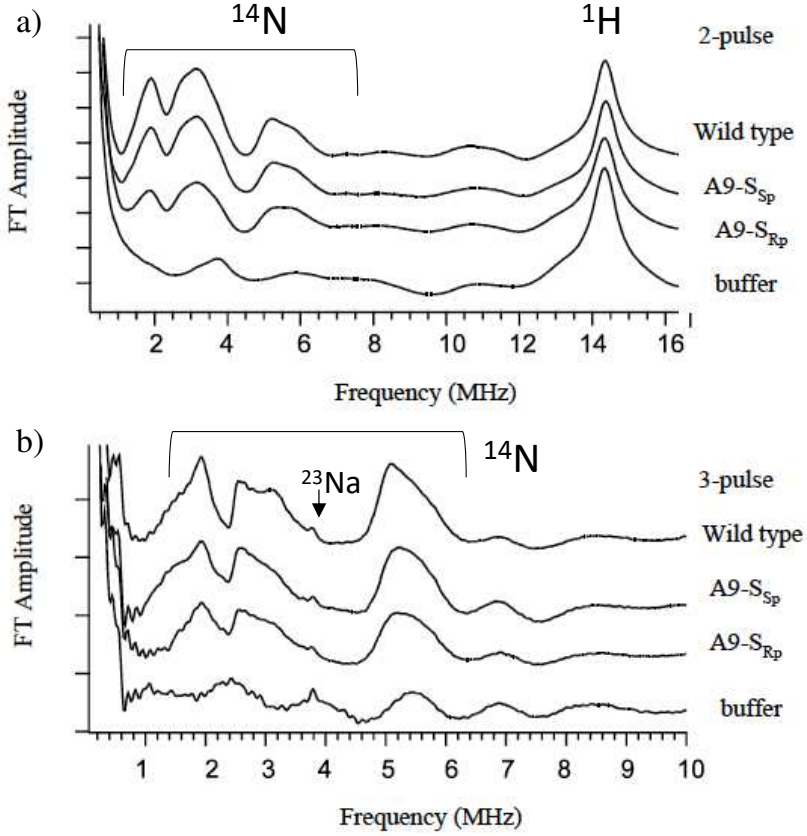

Figure 4. ESEEM spectra of 1:1 Mn^{2+}: tHHRz for wild-type, A9-S_{Sp}, A9-S_{Rp} samples, and Mn^{2+}-buffer control. a) Frequency domain showing ^{14}N and ^{1}H features in 2-pulse experiment comparing wild type, A9-S_{Sp}, A9-S_{Rp}, and buffer. b) 3-pulse experiment showing the ^{14}N region of wild type, A9-S_{Sp}, A9-S_{Rp}, and buffer. Modulation due to ^{23}Na in the buffer indicated by arrow. All samples in 5 mM TEA, pH 7.8, 1 M Na^+, 20% v/v ethylene glycol, 9.4 GHz, 3360 G, 4.2K.

EXAFS spectroscopy: Mn^{2+} does not coordinate sulfur in either A9-S_{Sp} or A9-S_{Rp} tHHRz

EXAFS spectroscopy was chosen to explore Mn^{2+} ligands in the hammerhead A9-S samples in an effort to determine the proximity of sulfur to the Mn^{2+} ion. EXAFS spectroscopy measures the effect of neighboring atoms on the metal ion X-ray absorption coefficient, an effect

that is sensitive to the distance, number, and type of neighboring ligands [43,44]. Since S has a larger scattering coefficient than O as well as longer metal-ligand bond lengths, the direct coordination of sulfur to Mn^{2+} and potentially second-sphere P, S, and O interactions should be detectable in an EXAFS experiment. EXAFS data at the Mn K-edge were obtained on Mn^{2+} in WT, A9-S$_{\mathit{R}}$p and A9-S$_{\mathit{S}}$p tHHRz samples. For comparison, EXAFS data were also obtained for model compounds Mn-ATP, Mn-GMP, and Mn-ATP-γS. In addition, Cd K-edge EXAFS data were obtained on Cd^{2+} bound to WT, A9-S$_{\mathit{R}}$p and A9-S$_{\mathit{S}}$p tHHRz samples.

Peaks in the EXAFS Fourier transform (FT) spectrum represent scattering from groups of atoms at a given average distance R (Å) from the metal ion. For the wild type tHHRz, the Mn^{2+} Fourier transform (FT) spectrum is dominated by a first-shell interaction at ~ 2.2 Å with a smaller feature(s) around 3 Å (Figure 5a). These data are best fit assuming a coordination environment with six light-atom scatterers (O or N) at a distance of 2.18 Å, three light-atom scatterers (C, N or O) at 3.06 Å and a heavier scatterer (S or P) at 3.49 Å (Fit 4; Table 1). Inclusion of the 3.49 Å (S, P) shell does not significantly improve the goodness-of-fit value (f') and the high Debye-Waller factor (DW) indicates that the shell has only a small contribution to the total EXAFS amplitude (*cf.* Fits 2,4; Table 1) for the WT tHHRz. This shell is included as a reference point for fits of A9-S$_{\mathit{S}}$p and A9-S$_{\mathit{R}}$p data (vide infra). If the Mn^{2+} coordinates to the guanine-N7, then the nitrogen (N7) along with putative water ligands [36] would contribute to the 2.2 Å shell. The ~ 3 Å shell would consist of C5, C6, and C8 from the guanine. The phosphodiester, bound in an end-on fashion through one oxygen, would result in a metal-phosphorus distance of 3.6-3.7 Å, which is not easily observed in these EXAFS data [45].

If Mn^{2+} binds to sulfur in the A9-S samples, a change in the first shell of scattering atoms is expected. Substitution of an oxygen ligand by a sulfur ligand, which should have a longer Mn-ligand distance, is expected to increase R by ~0.2 Å. The higher Z sulfur scatter should also slightly increase the peak amplitude. These effects are not observed in either of the A9-S samples. The Mn^{2+} EXAFS data of A9-S$_{\mathit{S}}$p exhibit a first-shell FT feature at ~ 2.2 Å that is like that of WT (Figure 5b). The A9-S$_{\mathit{S}}$p data are best fit assuming a similar coordination environment as wild type ribozyme with six light-atom scatterers at 2.21 Å, and three carbon atoms at 3.06 Å (Fit 8, Table 1). As with the WT sample, inclusion of a sulfur or phosphorus shell at 3.4 Å provides a slight improvement in f', though the DW factor is higher than would be expected. However, the FT feature appearing at > 3 Å is larger for A9-S_{Sp} than for the wild type

data. This increase is modeled as a decrease in the DW factor of both of the outer shells (*cf.* Fits 4,8; Table 1). The decrease in DW factor values may be explained by differences in the relative disorder of the sites, or by the presence of a non-coordinating S from the phosphorothioate.

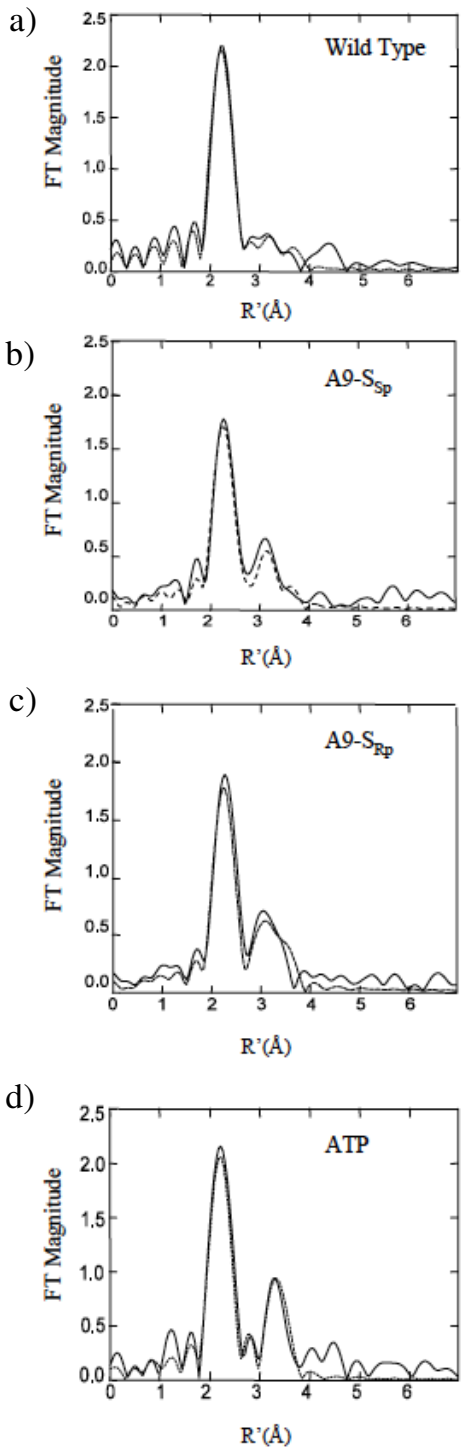

Figure 5. Mn EXAFS Fourier transforms (over the range of k = 2-11 Å^{-1}). (a) wild type ribozyme (solid) and the calculated spectra for Fit 4, Table 1 (dashed), (b) A9-S_{Sp} ribozyme (solid) and the calculated spectra for Fit 8, Table 1 (dashed), (c) A9-S_{Rp} ribozyme (solid) and the calculated spectra for Fit 12, Table 1 (dashed), (d) Mn-ATP (solid) and the calculated spectra for Fit 14, Table 1 (dashed).

The Mn^{2+} EXAFS data of A9-S_{Rp} also shows a large FT feature at ~ 2.2 Å, but has a more dominant feature at > 3 Å (Figure 5c). The best fit for the A9-S_{Rp} data requires 2 heavy atom scatterers in the outer shell at ~3.4 Å, in addition to the six O/N first-shell scatterers at 2.20 Å and three outer shell carbons at 3.01 Å (Fit 12; Table 1). In this case, the improvement to f' upon addition of the (S,P) outer shell is significant and the DW factor clearly indicates the importance of this shell to the total fit (*cf.* Fits 10,12; Table 1). A model that is consistent with these data includes a mode of coordination for the phosphorothioate that has both the sulfur and phosphorus at ~ 3.4 Å from the Mn^{2+}.

None of the fits for Mn EXAFS of the A9-S_{Sp} and A9-S_{Rp} tHHRz samples include sulfur coordination in the first shell. Thus, these data are conclusive that sulfur is not a direct ligand to Mn^{2+} in A9-S_{Sp} or A9-S_{Rp}. Because of multiple contributions to the second shell of scatterers at $\geq$ 3 Å, detecting S at this distance is less certain. However, comparison of the A9-S_{Sp} and A9-S_{Rp} data suggests that the S is within 3.5 Å of Mn^{2+} in the A9-S_{Rp} sample.

EXAFS spectroscopy of Mn-nucleotide model complexes

Figure 5d shows the EXAFS data for a 10:1 ATP:Mn (1 M Na^+) complex, which provides a model for Mn-phosphate coordination. The best fit for these data assumes six (O, N) scatterers at 2.15 Å and three P scatterers at 3.34 Å (Fit 14, Table 1). While the model suggests coordination to all 3 phosphates, other conformations are possible [46-49]; the EXAFS data also accommodate fits to 2 phosphates, for example. The Mn-ATP complex serves as a model for an expected Mn-phosphate distance of 3.3 Å, which is consistent with the Mn-P distance modeled for wild type and A9-S hammerhead samples.

EXAFS spectra for small model complexes containing Mn^{2+} and GMP (guanosine monophosphate) and ATP(γ)S (adenosine gamma-thiotriphosphate) were also obtained for additional comparison to the tHHRz data (Figure 6). In Mn-GMP, Mn^{2+} coordinates to the imino

N7 of guanine and has a through-water interaction with the 5′ phosphate. The FT of the Mn

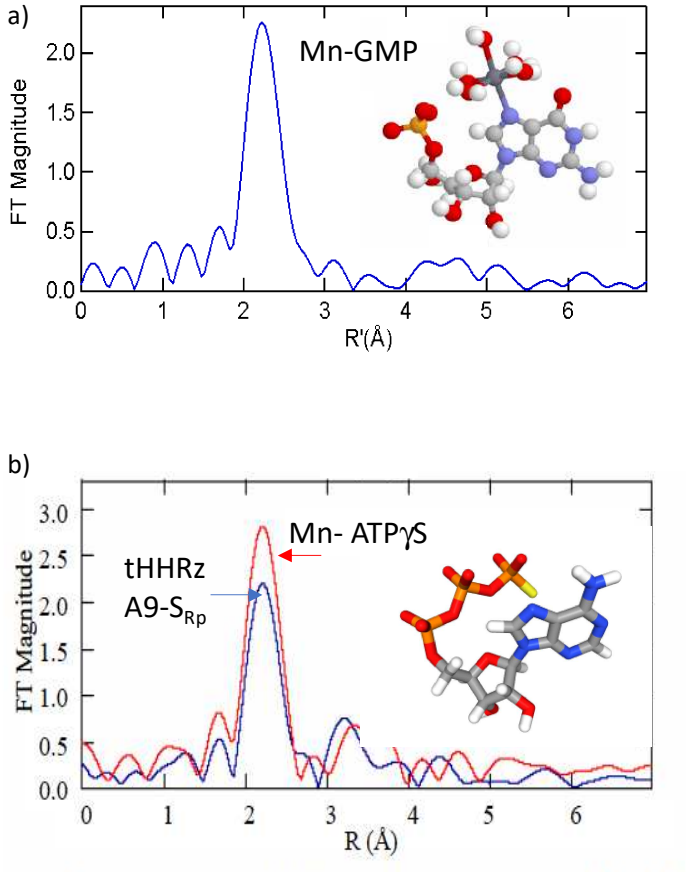

Figure 6. Mn EXAFS Fourier transforms (over the range of k = 2-11 Å^{-1}) for Mn-model compounds and tHHRz A9-S_{Rp} in $NaNO_3$. a) Mn-GMP (powdered sample). b) Mn-ATP(γ)S and tHHRz A9-S_{Rp} with $NaNO_3$ counterion. The ATPγS sample shows a broad feature at 3 Å similar to that observed for the tHHRz A9-S_{Rp} hammerhead sample. Replacement of Cl^- with NO_3^- counterions does not affect Mn EXAFS spectra for the tHHRz.

EXAFS results obtained on powdered Mn-GMP show mainly a single peak that is modeled as a first shell coordination sphere of 6 N/O backscatters at an average distance of 2.19 Å (Figure 6a and Table 2). These data are consistent with distances expected from the crystal structure of Mn-GMP (see Materials and Methods), and similar to the 1st shell scatterers in Mn-tHHRz. The EXAFS results for the Mn-GMP sample do not show any features at a distance of 3.4 Å as were observed in the hammerhead samples. This result supports assignment of the > 3 Å scatterers in the tHHRz to Mn-phosphodiester coordination, and not to multiple scattering effects from a single guanosine ring. The Mn-P distance in Mn-GMP of 4.9 Å, from the through-water

interaction to the 5'-monophosphate, would be expected to have a long-range scattering from P not observed in these EXAFS data.

As a possible model for a Mn-thiophosphate interaction, a Mn-ATP(γ)S (1:10) complex was prepared. The EXAFS results for the solution show a strong peak at 2.2 Å from an O/N shell and a somewhat broad feature at 3.4 Å that is consistent with a distant P atom (Figure 6b). The intensity of the 3.4 Å feature is lower in the Mn-ATP(γ)S sample than for the Mn-ATP complex, which may be due to more heterogeneous coordination in the ATPγS sample [49]. Consistent with prior studies, there is no direct evidence for the presence of a sulfur atom in the Mn^{2+} coordination sphere of Mn-ATP(γ)S [49].

Although the Mn EXAFS data do not support direct Mn-S coordination for any tHHRz sample, a further experiment was performed to check for the influence of high concentrations of NaCl that were used in sample preparation. Because S and Cl are difficult to distinguish by scattering potential, the presence of Cl ions either coordinated or nearby may influence the EXAFS spectrum. The EXAFS FT of a Mn-tHHRz A9-S_{Rp} sample prepared in 1 M $NaNO_3$, as opposed to the usual 1 M NaCl salt, is shown in Figure 6b in comparison with the Mn-ATPγS sample. The FT spectrum of this Mn-tHHRz A9-S_{Rp} $(NO_3)^-$ is very similar to that of the sample prepared in Cl- (Figure 5c), indicating that the counterion is not influencing these scatterers near the high-affinity Mn^{2+} tHHRz site.

EXAFS spectroscopy supports Cd-S coordination in both Cd- A9-S_{Sp} or A9-S_{Rp} tHHRz

Cd^{2+} rescues the activity of the Rp A9 phosphorothioate-modified hammerhead and has previously been suggested, based on ^{31}P NMR studies, to coordinate to the sulfur atom in both the R_p and S_p isomers [14]. Here, EXAFS spectroscopy was performed to confirm these predicted Cd-S interactions for the tHHRz. In comparison with Cd-WT tHHRz samples, the Cd K-edge absorption energy is decreased in both Cd- A9-S_{Rp} and -S_{Sp} samples (Figure 7a), consistent with replacement of an O ligand with a higher electron density S coordination. The EXAFS results for the Cd-WT tHHz sample showed an intense FT feature at 2.40 Å (Figure 7b) that is modeled with 6 N/O atoms at 2.40 Å (Table 2). This Cd-O/N distance is ~0.2 Å longer than the predicted Mn-O scatterers, as expected for the larger Cd^{2+} ion. The EXAFS FT features for the A9 R_p and S_p isomers have a greater intensity of the peak at 2.4 Å and a slight shift to a longer average distance (Figure 7b). The fits for both the A9-S_{Rp} and -S_{Sp} samples (Table 2) suggest a shell of

five O/N atoms at 2.4 Å and a S atom at 2.6 Å. These results are consistent with direct coordination of the Cd^{2+} ion to sulfur in both isomers of the A9 phosphorothioate substitution in the tHHRz.

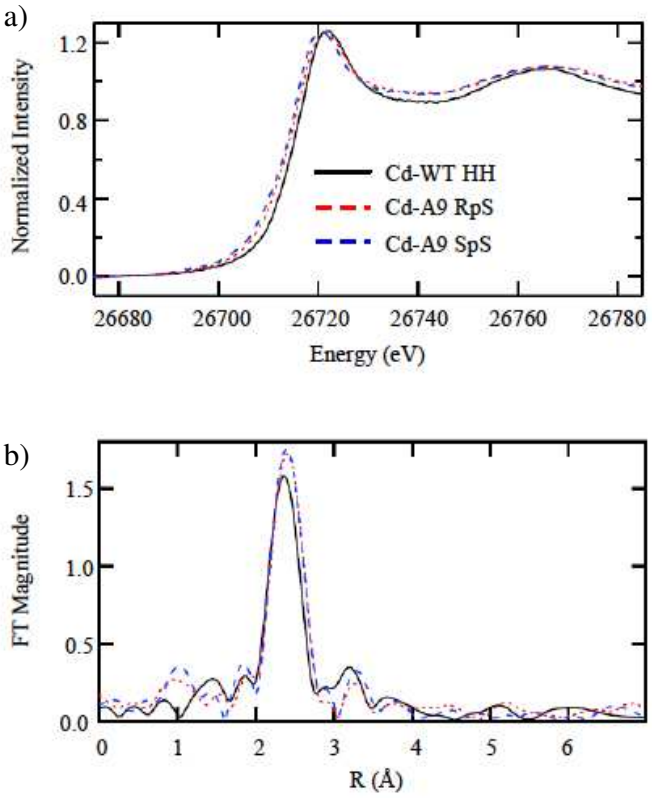

Figure 7. Cd K-edge and EXAFS Fourier transforms (over the range of k = 2-11 $Å^{-1}$) for wild type, A9-S_{Sp} and A9-S_{Rp} tHHRz. a) The Cd X-ray absorption edge is slightly lower for the tHHRz A9-S samples (dashed). b) Longer distance and higher amplitude for first-shell scatterers in both of the tHHRz A9-S samples (dashed).

Computational analysis of metal-O/S coordination in a thiophosphate model system

The spectroscopic data described above indicate that for both isomers of an A9 phosphorothioate in the tHHRz, Mn^{2+} preferentially coordinates to the oxygen ligand whereas Cd^{2+} coordinates to sulfur. Computational modeling was used in order to further understand the relative stabilities of Mn^{2+}-O vs. Mn^{2+}-S coordination in thiophosphates. To model these interactions, Mn^{2+} and Cd^{2+} complexes with dimethylthiophosphate (DMPS), guanine, and aqua ligands were built and geometrically equilibrated. Consistent with prior predictions [51-54], the S atom carries a majority of the distributed negative charge in the uncoordinated DMPS anion

(Figure 8). As shown in Figure 8, the relative stabilities of Mn coordination to the O or S were assessed in equilibrated Mn^{2+} models. The total energy of each model includes contributions from the Mn-O/S bond as well as hydrogen-bonding interactions between the non-bonded DMPS O/S and one of the axial Mn-aqua ligands. Mn^{2+} coordination to O results in a markedly more stable complex (ΔE=-3.6 kcal/mol), consistent with the observation that Mn^{2+} coordinates to the oxygen ligand in both A9-S_{Rp} and -S_{Sp} tHHRz samples.

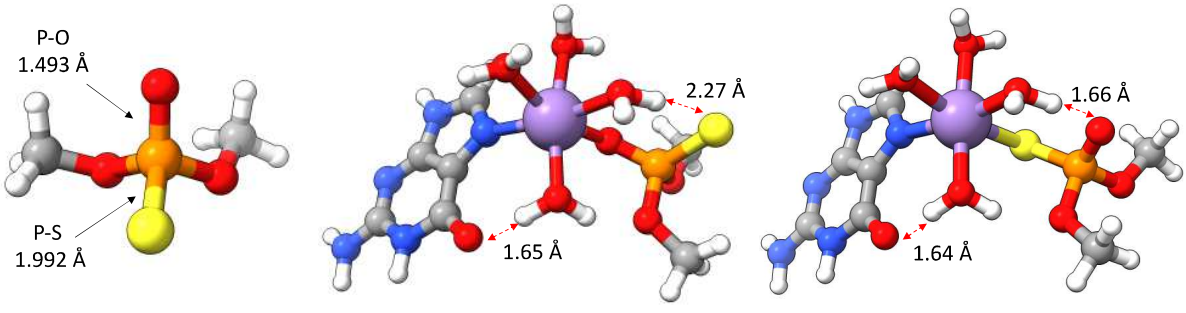

DMPS⁻

Non-bridging atom	Charge density (a.u.)
O	-0.67
S	-0.74
P	0.77

Mn - O

Relative energy = -3.6 kcal/mol

Non-bridging atom	Charge density (a.u.)
O	-0.62
S	-0.63
P	0.90
Mn	0.99

Mn - S

Relative energy = 0 kcal/mol

Non-bridging atom	Charge density (a.u.
O	-0.64
S	-0.55
P	0.89
Mn	0.92

Figure 8. Computational analysis demonstrates lower relative energy with Mn-O coordination in thiophosphate model systems. Selected bond distances and Mulliken charge densities are shown.

By contrast, equilibrated thiophosphate models built with Cd^{2+} were more stable with Cd-S coordination (Figure S5, ΔE=-6.2 kcal/mol), consistent with preferential soft Lewis acid, soft Lewis base interactions [55]. This could also influence Cd-substitution in biomolecular systems albeit in context of more constrained chelating environments [14]. Taken together, the results of computational modeling support the experimental observation that Mn^{2+} preferentially coordinates to the O-ligand of a phosphorothioate.

Molecular models for metals in the phosphorothioate-substituted tHHRz A9/G10.1 site

To investigate possible structural influences of metal coordination to either the pro-R_p or pro-S_p positions of the A9 phosphorothioate in the tHHRz A9/G10.1 site, molecular models were developed that take into consideration the results of the ESEEM and EXAFS data for metals at

that site in the tHHRz. A minimal model consisting of G8, A9, and G10.1 excised from the tHHRz crystal structure (PDB 1HMH [26]) was constructed (see Materials and Methods) and energy-minimized structures with bound metal ions and A9-S_{Rp} or -S_{Sp} substitutions were explored (Figure 9). The resulting structures with Mn^{2+} ion coordinated to the oxygen of WT or A9-S_{Sp} models (Figures 9A, C) are similar with respect to the disposition of the nucleobases, as is the model of Cd^{2+} bound to the S in A9-S_{Sp} (Figure 9B). By contrast, when Mn is modeled bound to the non-sulfur oxo group of the A9-S_{Rp} construct, the minimized structure shows significant rearrangement due to a change in torsion angles around the phosphorothioate bond. In the full tHHRz, this type of coordination may result in a conformational change in the phosphodiester backbone relative to wild type and A9-S_{Sp}, and may be the cause of the deleterious effect of the A9-S_{Rp} substitution on hammerhead ribozyme activity.

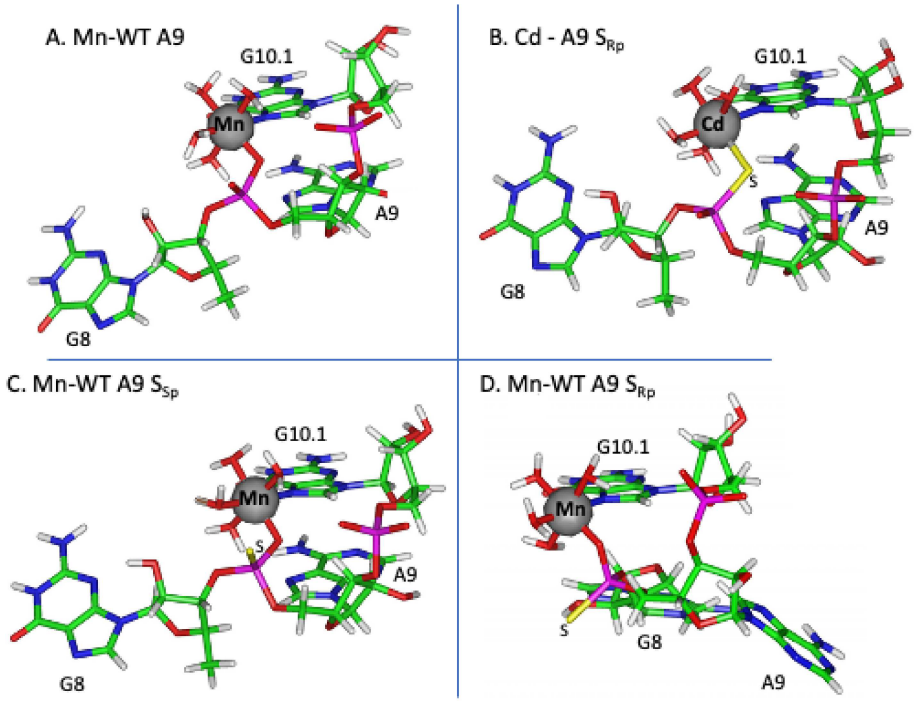

Figure 8. Proposed models for the A9/G10.1 metal coordination in the WT and thiophosphate-substituted hammerhead ribozyme based on EPR, ESEEM, and EXAFS experiments: (a) Mn-wild type, (b) Cd-A9-S_{Rp} (S coordination), (c) Mn-A9-S_{Rp} (O coordination), (d) Mn-A9-S_{Rp} (O coordination). An altered conformation in the Mn- A9-S_{Rp} sample is predicted to cause a structural effect that reduces hammerhead activity.

Discussion

In order to better understand how cations influence function in catalytic RNA, it is important to probe the cation binding sites in molecular detail. To this end, we have explored the A9/G10.1 metal ion site in the unmodified and A9-phosphorothioate-substituted truncated hammerhead ribozyme using several spectroscopic techniques. Previous results from PS-rescue experiments, with rescue provided by thiophilic Cd^{2+}, have supported the model that functional metals bind specifically to the pro-R_p oxygen of the A9 phosphate, or to sulfur in the R_p thiophosphate [14,22,24,26]. Here, we find through EPR and ESEEM experiments that Mn^{2+}, often used to rescue PS substitutions, does indeed bind to the A9-S site. However, while activity is not significantly changed for the A9-S_{Sp} sample, Mn^{2+} does not support activity when bound to the A9-S_{Rp} isomer. A rationale for this apparent discordance between structural and functional data is provided by EXAFS data, which show that Mn^{2+} does not directly coordinate to the S ligand in A9-S_{Rp} although the S appears to be held within 3.5 Å of the Mn^{2+} ion. Thus, a simple model that fits these data is that with an R_p phosphorothioate substitution at A9, Mn^{2+} prefers to coordinate to the nonbridging *oxygen* ligand of the thio-substituted phosphate.

Although Mn^{2+} is more thiophilic than Mg^{2+}, Mn^{2+} is still an oxophilic metal ion with an estimated ~10^2 higher affinity for oxygen over sulfur in a thiophosphate [55]. When an oxygen ligand is in proximity, as in a phosphorothioate, a rigid RNA structure around the metal ion site may be required in order to force Mn^{2+} coordination to sulfur. It appears that the hammerhead A9/G10.1 site, although a high-affinity metal ion site, has sufficient flexibility to support the oxophilic nature of Mn^{2+}. However, Mn^{2+} bound to the oxygen ligand of the R_p thiophosphate may cause a distortion in the RNA structure that has dramatic, negative consequences for activity. By contrast, the EXAFS data show that the larger and more thiophilic Cd^{2+} ion binds to the sulfur of the R_p thiophosphate; this interaction supports HHRz activity. These results demonstrate that the structure around the A9/G10.1 site is critical to hammerhead ribozyme activity, wherein a small change in metal ion coordination can cause very large changes in chemical activity.

The results found here suggest a modification in one premise of the popular PS-rescue experiments. It is commonly concluded that when a PS-substitution results in a reversible knockout of Mg^{2+}-dependent activity, the lack of activity is caused because Mg^{2+} no longer binds to the sulfur-substituted site. Instead, we suggest that it is also possible that the oxophilic Mg^{2+}

ion may indeed still bind in the metal ion site, but to the *oxo* ligand of the substituted site, causing an inhibitory distortion of the ribozyme structure. Although a subtle distinction, this hypothesis may change the molecular details of interpreting PS-rescue experiments. There have been only a few structural characterizations of phosphorothioate-modified nucleic acids, but these studies, including the one presented here, demonstrate that each thiophosphate modification must be considered as unique in PS rescue experiments [4,9-15].

The ability of Mn^{2+} to rescue activity following phosphorothioate substitutions in several different RNAs has been ascribed to its higher affinity for sulfur than that of Mg^{2+} [56-58]. In some cases, notably the cleavage site of the hammerhead ribozyme, Mn^{2+} is able to rescue activity in a PS-substituted site [56]. Several scenarios accommodate such results. In one scenario, the substituted site is indeed rigid with additional metal coordination sites, and it is energetically favorable for the rescuing Mn^{2+} to bind to sulfur, as is observed in Mn-thiolate model compounds [59,60]. Another possibility is that the sulfur substitution causes distortion that lowers overall metal ion affinity for that site, but some compensating property of Mn^{2+} such as the higher affinity of Mn^{2+} over Mg^{2+} for O/N RNA sites in general [50] or phosphodiester ligands in particular [16] overcomes the negative effect. Interestingly, both thiophilic Hg^{2+} [63] and Cd^{2+} [14,64] have also been demonstrated spectroscopically to bind to the tHHRz cleavage site. There is also a possibility that Mn^{2+} rescue may occur due to binding to a site other than that substituted in the PS-rescue experiment [62]. Given these complexities as well as the prediction here that Mn^{2+} binding to a phosphorothioate oxygen may induce structural distortion, the distinctively thiophilic Cd^{2+} might be encouraged as a better test for a metal site in the PS-rescue experiment.

The data presented here suggest a modification of the simple picture of RNA metal sites that are uncovered by PS-rescue experiments, but do not diminish the PS-rescue experiment as a powerful technique for predicting metal ion sites in RNA. In the case of the hammerhead ribozyme A9/G10.1 site, originally identified as functionally important using phosphorothioates, we previously monitored Mn^{2+} coordination through EPR methods [35,36,38,40], Cd^{2+} binding to the PS-substituted A9 site by ^{31}P NMR [14], and now have explored Mn^{2+} coordination to the PS-substituted site. Combining spectroscopy with mechanistic studies has provided a more detailed picture of this functionally-critical metal ion site.

Materials and Methods

RNA samples of the truncated HHRz (tHHRz) were prepared with the sequences in Fig. 1. For spectroscopic studies, a C13 2′-OMe substitution in the substrate strand was included to inhibit cleavage. The WT and 13-O-methyl substrate strands, 34-nucleotide enzyme strand with a phosphorothioate 5′ to A9 (mixed diastereomers), and WT enzyme strand were purchased (Dharmacon Research, Lafayette, CO) and deprotected just before purification according to manufacturer protocols. The RNA purification included separating the correct length of RNA on 20% acrylamide gels, followed by electroelution, and dialysis against buffers (5 mM TEA, pH 7.8, 100 mM NaCl or 10 mM MOPS, pH 7.0, 100 mM NaCl) as described previously [34]. $NaNO_3$ was substituted in some experiments to rule out an influence of Cl^- on EXAFS results. Unless noted, chemicals were obtained from Sigma.

The hammerhead ribozyme complexes were formed by heating a 1:1 complex of enzyme and substrate to 90° for 2-3 minutes and cooling on ice for 30 minutes. Samples for EPR, ESEEM, and EXAFS were made by adding one equivalent of Mn^{2+} or Cd^{2+} to the enzyme-substrate complex after cooling. Mn^{2+} and Cd^{2+} were added to the hammerhead as buffered metal solutions that were made daily from 1 M stock solutions. The $MnCl_2$ 1 M solution was purchased as 1 mL aliquots. $Mn(NO_3)_2$ and $CdCl_2$ in water were prepared from salts.

The buffer used in all the spectroscopic experiments was 5 mM TEA, pH 7.8, 1 M NaCl (or $NaNO_3$), with 20 % (v/v) ethylene glycol as cryoprotectant. The buffer used in the activity studies was 10 mM MOPS, pH 7.0, 1 M NaCl. The activity studies were performed as described previously [34] but at lower pH to maximize the range of measurable rates as well as enhance solubility of Cd^{2+}.

Separation of phosphorothioate isomers of A9-S enzyme strand

The chemically synthesized A9-phosphorothioate-substituted enzyme strand (Dharmacon) contains a mixture of R_p and S_p diastereomers. The diastereomers were separated based on the technique reported by Slim & Gait [65,14]. The separation was achieved using reverse phase HPLC (Äkta Purifier, Pharmacia) on a C18 column (5μ 6.3/250, Pharmacia) fitted with a guard column (Upchurch, Oak Harbor, WA). The buffer system was 0.1 M ammonium acetate stationary phase (Buffer A) and 80% acetonitrile/20% 0.1 M ammonium acetate mobile phase (Buffer B). The gradient was greatly extended to facilitate the separation of the longer

RNA. The elution gradient is composed of 3 parts, 0-5% B over 8 column volumes (CV), 5-12% B over 90 CV, 12-50% B over 1 CV, followed by a cleaning of the column with 2 CV 50% B, and then a re-equilibration with Buffer A. Fractions were collected from 5.3% to 13% B and the full-length RNA eluted with two major peaks corresponding to the R_p and S_p isomers at ~7 % and ~7.6 % B respectively. The fractions from each of the separate peaks were pooled together and reduced in volume by rotary-evaporation, dialyzed, concentrated, and ethanol precipitated. The configuration of the isomers (R_p versus S_p) was determined by treatment with snake venom phosphodiesterase digestion as described previously [14,65] and verified by activity studies since the R_p isomer is reported to show a 500 to 10,000- fold decrease in tHHRz activity in Mg^{2+} whereas the S_p isomer shows little effect on activity [24]. ^{31}P NMR confirmed diastereomeric purity as shown previously [14]. In general, the solid phase synthesis produced an excess of R_p (~65%) versus S_p (35%) isomers.

Mn-GMP crystals were prepared as previously described [66] and the structure verified by X-ray crystallography (Dr. Joseph Reibenspies at the X-ray Diffraction Laboratory, Center for Chemical Characterization and Analysis, Texas A&M University). The complex crystallizes in a monoclinic system with the space group C2. The Mn^{2+} ion is surrounded by five H_2O molecules at an average Mn-O distance of 2.2 Å and is coordinated to the N7 position of the guanine residue with a Mn-N distance of 2.250(8) Å. A Mn- ATP(γ)S (BioMol) complex in a 1 to 10 ratio was prepared in a 10 mM boric acid buffer at pH 8.

Low temperature EPR

EPR measurements were performed on an X-band Bruker ESP-300 spectrometer equipped with an Oxford liquid helium cryostat. Samples of 60-75 µL 1:1 Mn^{2+}: RNA (200-400 µM RNA) were measured using quartz capillary tubes purchased from Wilmad Glass (i.d. = 2.0 mm, o.d. = 2.4 mm). Typical EPR acquisition parameters are 10 K, 0.063 mW microwave power, 15 G p.t.p. 100 kHz field modulation, and 6.1 G/sec scan rate.

ESEEM

ESEEM spectroscopy was performed on a laboratory built 8-18 GHz spectrometer described previously [67,68]. Two- and three- pulsed ESEEM experiments were performed as previously described [41]. In the 3-pulse experiments, tau was chosen to be an integral multiple of the ^1H precession frequency (210 ns) to cancel weakly coupled proton modulation. All

spectra were taken at 4.2K. ESEEM samples (400 μM to 1 mM) were placed in precision quartz tubes (706-PQ-9.05) (Wilmad, Buena, NJ).

EXAFS

EXAFS samples (1.1 mM) of ribozyme and ATP (10 mM), with 20% ethylene glycol as a glassing agent, were frozen in polycarbonate cuvettes, 24x3x1 mm with a 0.025 mm Mylar window covering one 24x3 mm face. XAS data were collected at Stanford Synchrotron Radiation Laboratory (SSRL) with the SPEAR storage ring operating in a dedicated mode at 3.0 GeV (See Supplementary Material, Table S1). The edge spectra for multiple scans obtained on the same sample did not change, indicating that the samples were not damaged by exposure to X-ray radiation. EXAFS analysis was performed using EXAFSPAK software (www-ssrl.slac.stanford.edu/exasfspak.html), according to standard procedures [43]. Both single- and multiple-scattering from the Mn were used to identify and quantify coordination of phosphate. Multiple-scattering paths were built by importing the crystal structure of Mn-ATP into Chem3D (Cambridge Scientific). The structure was edited to only the Mn^{2+} and one phosphate and the coordinates were imported to FEFF v. 7.02 [69] to calculate scattering amplitudes and paths for each scattering path containing four or fewer legs.

Computational analysis of metal-O/S coordination

Electronic structure modeling: Model systems were created in Avogadro, with the phosphorothioate terminated with methyl groups. All structures were geometrically and electronically equilibrated using a hybrid GGA functional with a triple zeta basis (B3LYP/Def2TZVP), as implemented in Gaussian09. Convergence was set to 4.5 x 10^{-4} Ha and 1.8 x 10^{-3} Å for atomic forces and displacements, respectively. Several isomers of O/S bound phosphorothioate ligands were calculated and the lowest energy structures were compared. The Mn structures were run as a sextet. A solvent cavity reaction field was employed to approximate liquid water, using a polarizable continuum. Mulliken charge analysis was performed to parse the charge density.

Molecular mechanics modeling: A molecular mechanics approach was used to model the structural perturbation promoted by metal ions bound at the A9/G10.1 site in the hammerhead ribozyme. Initial models were constructed from PDB: 1HMH [26] by deleting all bases except G8, A9, and G10.1. The Mn^{2+} ion was modeled coordinated to the N7 position of G10.1 and the pro-R_p oxygen of the A9 phosphate with four water molecules filling out the coordination sphere.

Models were capped with a H at the 3′ end and a methyl group at the 5′ end. For phosphorothioate models, a single sulfur atom was substituted for one of the non-bridging oxygen atoms of A9 phosphate in either in the R_p or S_p position. Experiments were also performed with a Cd^{2+} ion replacing the Mn^{2+} ion in the non-sulfur and sulfur substituted A9/G10.1 models. The potential of each atom was assigned with UFF and the energy of the structure was minimized using the Smart Minimizer energy minimization method in the program Cerius2 (Accelrys) operating under Unix.

Acknowledgements

This research was supported by the National Institutes of Health (GM58096 (VJD), GM61211 (RDB), and GM42025 (RAS)), the NSF (CHE-0111696 and CHE 210955 (VJD), MCB 2018296 (CGH), and CHE0092010 for TAMU EPR facilities), and the Robert A. Welch Foundation (VJD). AMD and CHH were supported by The Research Corporation for Science Advancement (Cottrell Scholar Program) for non-tenured faculty. Computational studies were performed by using the High-Performance Computing cluster at the University of Oregon (Talapas) and the Extreme Science and Engineering Discovery Environment (XSEDE), which is supported by National Science Foundation Grant ACI-1548562. Portions of this research were carried out at the Stanford Synchrotron Radiation Laboratory (SSRL), a national user facility operated by Stanford University on behalf of the U. S. Department of Energy, Office of Basic Energy Sciences. The SSRL Structural Molecular Biology Program is supported by the Department of Energy, Office of Biological and Environmental Research, and by the National Institutes of Health, National Center for Research Resources, Biomedical Technology Program.

References

[1] Ward, W. L.; Plakos, K.; DeRose, V. J. Nucleic Acid Catalysis: Metals, Nucleobases, and Other Cofactors. *Chem. Rev.* **2014**, *114* (8), 4318–4342. https://doi.org/10.1021/cr400476k

[2] Donghi, D.; Schnabl, J. Multiple Roles of Metal Ions in Large Ribozymes. *Met. Ions Life Sci.* **2011**, *9*, 197–234. https://doi.org/10.1039/9781849732512-00197.

[3] DeRose, V. J.; Yglesias, M. V. 8.39 - Metal Ion Interactions With DNA, RNA, and Nucleic Acid Enzymes. In *Comprehensive Coordination Chemistry III*; Constable, E. C., Parkin, G., Que Jr, L., Eds.; Elsevier: Oxford, 2021; pp 968–993. https://doi.org/10.1016/B978-0-08-102688-5.00112-4.

[4] Frederiksen, J. K.; Piccirilli, J. A. Identification of Catalytic Metal Ion Ligands in Ribozymes. *Methods* **2009**, *49* (2), 148–166. https://doi.org/10.1016/j.ymeth.2009.07.005.

[5] Saran, R.; Huang, Z.; Liu, J. Phosphorothioate Nucleic Acids for Probing Metal Binding, Biosensing and Nanotechnology. *Coordination Chemistry Reviews* **2021**, *428*, 213624. https://doi.org/10.1016/j.ccr.2020.213624.

[6] Eckstein, F. Phosphorothioates, Essential Components of Therapeutic Oligonucleotides. *Nucleic Acid Therapeutics* **2014**, *24* (6), 374–387. https://doi.org/10.1089/nat.2014.0506.

[7] (a) Hyjek-Składanowska, M.; Vickers, T. A.; Napiórkowska, A.; Anderson, B. A.; Tanowitz,M.; Crooke, S. T.; Liang, X.; Seth, P. P.; Nowotny, M. Origins of the Increased Affinity of Phosphorothioate-Modified Therapeutic Nucleic Acids for Proteins. *J. Am. Chem. Soc.* **2020**, *142* (16), 7456–7468. https://doi.org/10.1021/jacs.9b13524. (b) Warminski, M.; Kowalska, J.; Nowak, E.; Kubacka, D.; Tibble, R.; Kasprzyk, R.; Sikorski, P. J.; Gross, J. D.; Nowotny, M.; Jemielity, J. Structural Insights into the Interaction of Clinically Relevant Phosphorothioate MRNA Cap Analogs with Translation Initiation Factor 4E Reveal Stabilization via Electrostatic Thio-Effect. *ACS Chem. Biol.* **2021**, *16* (2), 334–343. https://doi.org/10.1021/acschembio.0c00864.

[8] Brautigam, C. A.; Steitz, T. A. Structural Principles for the Inhibition of the 3'-5' Exonuclease Activity of Escherichia Coli DNA Polymerase I by Phosphorothioates. *J Mol Biol* **1998**, *277* (2), 363–377. https://doi.org/10.1006/jmbi.1997.1586.

[9] Zhang, Z.; Vögele, J.; Mráziková, K.; Kruse, H.; Cang, X.; Wöhnert, J.; Krepl, M.; Šponer, J. Phosphorothioate Substitutions in RNA Structure Studied by Molecular Dynamics Simulations, QM/MM Calculations, and NMR Experiments. *J. Phys. Chem. B* **2021**, *125* (3), 825–840. https://doi.org/10.1021/acs.jpcb.0c10192.

[10] Reiter, N.J.; Nikstad, L.J.; Allmann, A.M.; Johnson, R.J.; Butcher, S.E. Structure of the U6 RNA Intramolecular Stem–Loop Harboring an SP-Phosphorothioate Modification. *RNA* **2003**, *9* (5), 533–542. https://doi.org/10.1261/rna.2199103.

[11] Smith, J. S.; Nikonowicz, E. P. Phosphorothioate Substitution Can Substantially Alter RNA Conformation. *Biochemistry* **2000**, *39* (19), 5642–5652. https://doi.org/10.1021/bi992712b.

[12] Bonneau, E.; Legault, P. NMR Localization of Divalent Cations at the Active Site of the Neurospora VS Ribozyme Provides Insights into RNA–Metal-Ion Interactions. *Biochemistry* **2014**, *53* (3), 579–590. https://doi.org/10.1021/bi401484a.

[13] Erat, M. C.; Besic, E.; Oberhuber, M.; Johannsen, S.; Sigel, R. K. O. Specific Phosphorothioate Substitution within Domain 6 of a Group II Intron Ribozyme Leads to Changes in Local Structure and Metal Ion Binding. *JBIC Journal of Biological Inorganic Chemistry* **2018**, *23* (1), 167–177. https://doi.org/10.1007/s00775-017-1519-3.

[14] Maderia, M.; Hunsicker, L. M.; DeRose, V. J. Metal–Phosphate Interactions in the Hammerhead Ribozyme Observed by ^{31}P NMR and Phosphorothioate Substitutions. *Biochemistry* **2000**, *39* (40), 12113–12120. https://doi.org/10.1021/bi001249w.

[15] (a) Thaplyal, P.; Ganguly, A.; Golden, B. L.; Hammes-Schiffer, S.; Bevilacqua, P. C. ThioEffects and an Unconventional Metal Ion Rescue in the Genomic Hepatitis Delta Virus Ribozyme. *Biochemistry* **2013**, *52* (37), 6499–6514. https://doi.org/10.1021/bi4000673. (b) Ganguly, A.; Weissman, B. P.; Giese, T. J.; Li, N.-S.; Hoshika, S.; Rao, S.; Benner, S. A.; Piccirilli, J. A.; York, D. M. Confluence of Theory and Experiment Reveals the Catalytic Mechanism of the Varkud Satellite Ribozyme. *Nature Chemistry* **2020**, *12* (2), 193–201. https://doi.org/10.1038/s41557-019-0391-x.

[16] Knobloch, B.; Nawrot, B.; Okruszek, A.; Sigel, R. K. O. Discrimination in Metal-Ion Binding to RNA Dinucleotides with a Non-Bridging Oxygen or Sulfur in the Phosphate Diester Link. *Chemistry – A European Journal* **2008**, *14* (10), 3100–3109. https://doi.org/10.1002/chem.200701491.

[17] Forster, A. C.; Symons, R. H. Self-Cleavage of Virusoid RNA Is Performed by the Proposed 55-Nucleotide Active Site. *Cell* **1987**, *50* (1), 9–16. https://doi.org/10.1016/0092-8674(87)90657-X.

[18] Blount, K. F.; Uhlenbeck, O. C. The Structure-Function Dilemma of the Hammerhead Ribozyme. *Annu. Rev. Biophys. Biomol. Struct.* **2005**, *34* (1), 415–440. https://doi.org/10.1146/annurev.biophys.34.122004.184428.

[19] Hutchins, C. J.; Rathjen, P. D.; Forster, A. C.; Symons, R. H. Self-Cleavage of plus and Minus RNA Transcripts of Avocado Sunblotch Viroid. *Nucleic Acids Research* **1986**, *14* (9), 3627–3640. https://doi.org/10.1093/nar/14.9.3627.

[20] Prody, G. A.; Bakos, J. T.; Buzayan, J. M.; Schneider I. R.; Bruening G. Autolytic Processing of Dimeric Plant Virus Satellite RNA. *Science* **1986**, *231* (4745), 1577–1580. https://doi.org/10.1126/science.231.4745.1577.

[21] Martick, M.; Horan, L. H.; Noller, H. F.; Scott, W. G. A Discontinuous Hammerhead Ribozyme Embedded in a Mammalian Messenger RNA. *Nature* **2008**, *454* (7206), 899–902. https://doi.org/10.1038/nature07117.

[22] Osborne, E.M., Schaak, J.E., DeRose, V.J. Characterization of a Native Hammerhead Ribozyme Derived from Schistosomes. *RNA* **2005**, *11* (2), 187–196. https://doi.org/10.1261/rna.7950605.

[23] Kim, N.-K.; Murali, A.; DeRose, V. J. Separate Metal Requirements for Loop Interactions and Catalysis in the Extended Hammerhead Ribozyme. *J. Am. Chem. Soc.* **2005**, *127* (41), 14134–14135. https://doi.org/10.1021/ja0541027.

[24] Wang, S.; Karbstein, K.; Peracchi, A.; Beigelman, L.; Herschlag, D. Identification of the Hammerhead Ribozyme Metal Ion Binding Site Responsible for Rescue of the Deleterious Effect of a Cleavage Site Phosphorothioate. *Biochemistry* **1999**, *38* (43), 14363–14378. https://doi.org/10.1021/bi9913202.

[25] Peracchi, A.; Beigelman, L.; Scott, E. C.; Uhlenbeck, O. C.; Herschlag, D. Involvement of a Specific Metal Ion in the Transition of the Hammerhead Ribozyme to Its Catalytic Conformation. *Journal of Biological Chemistry* **1997**, *272* (43), 26822–26826. https://doi.org/10.1074/jbc.272.43.26822.

[26] Pley, H. W.; Flaherty, K. M.; McKay, D. B. Three-Dimensional Structure of a Hammerhead Ribozyme. *Nature* **1994**, *372* (6501), 68–74. https://doi.org/10.1038/372068a0.

[27] Murray, J. B.; Terwey, D. P.; Maloney, L.; Karpeisky, A.; Usman, N.; Beigelman, L.; Scott, W. G. The Structural Basis of Hammerhead Ribozyme Self-Cleavage. *Cell* **1998**, *92* (5), 665–673. https://doi.org/10.1016/S0092-8674(00)81134-4.

[28] Mir, A.; Chen, J.; Robinson, K.; Lendy, E.; Goodman, J.; Neau, D.; Golden, B. L. Two Divalent Metal Ions and Conformational Changes Play Roles in the Hammerhead Ribozyme Cleavage Reaction. *Biochemistry* **2015**, *54* (41), 6369–6381. https://doi.org/10.1021/acs.biochem.5b00824.

[29] Mir, A.; Golden, B. L. Two Active Site Divalent Ions in the Crystal Structure of the Hammerhead Ribozyme Bound to a Transition State Analogue. *Biochemistry* **2016**, *55* (4), 633–636. https://doi.org/10.1021/acs.biochem.5b01139.

[30] Chen, H.; Giese, T. J.; Golden, B. L.; York, D. M. Divalent Metal Ion Activation of a Guanine General Base in the Hammerhead Ribozyme: Insights from Molecular Simulations. *Biochemistry* **2017**, *56* (24), 2985–2994. https://doi.org/10.1021/acs.biochem.6b01192.

[31] Seith, D. D.; Bingaman, J. L.; Veenis, A. J.; Button, A. C.; Bevilacqua, P. C. Elucidation of Catalytic Strategies of Small Nucleolytic Ribozymes from Comparative Analysis of Active Sites. *ACS Catal.* **2018**, *8* (1), 314–327. https://doi.org/10.1021/acscatal.7b02976.

[32] Martick, M.; Scott, W. G. Tertiary Contacts Distant from the Active Site Prime a Ribozyme for Catalysis. *Cell* **2006**, *126* (2), 309–320. https://doi.org/10.1016/j.cell.2006.06.036.

[33] Ward, W. L.; DeRose, V. J. Ground-State Coordination of a Catalytic Metal to the Scissile Phosphate of a Tertiary-Stabilized Hammerhead Ribozyme. *RNA* **2012**, *18* (1), 16–23. https://doi.org/10.1261/rna.030239.111.

[34] Horton, T. E.; Clardy, D. R.; DeRose, V. J. Electron Paramagnetic Resonance Spectroscopic Measurement of Mn^{2+} Binding Affinities to the Hammerhead Ribozyme and Correlation with Cleavage Activity. *Biochemistry* **1998**, *37* (51), 18094–18101. https://doi.org/10.1021/bi981425p.

[35] Morrissey, S. R.; Horton, T. E.; DeRose, V. J. Mn^{2+} Sites in the Hammerhead Ribozyme Investigated by EPR and Continuous-Wave Q-Band ENDOR Spectroscopies. *J. Am. Chem. Soc.* **2000**, *122* (14), 3473–3481. https://doi.org/10.1021/ja992989z.

[36] Morrissey, S. R.; Horton, T. E.; Grant, C. V.; Hoogstraten, C. G.; Britt, R. D.; DeRose, V. J. Mn^{2+} –Nitrogen Interactions in RNA Probed by Electron Spin–Echo Envelope Modulation Spectroscopy: Application to the Hammerhead Ribozyme. *J. Am. Chem. Soc.* **1999**, *121* (39), 9215–9218. https://doi.org/10.1021/ja9921571.

[37] Schiemann, O.; Fritscher, J.; Kisseleva, N.; Sigurdsson, S. T.; Prisner, T. F. Structural Investigation of a High-Affinity MnII Binding Site in the Hammerhead Ribozyme by EPR Spectroscopy and DFT Calculations. Effects of Neomycin B on Metal-Ion Binding. *Chembiochem* **2003**, *4* (10), 1057–1065. https://doi.org/10.1002/cbic.200300653.

[38] Vogt, M.; Lahiri, S.; Hoogstraten, C. G.; Britt, R. D.; DeRose, V. J. Coordination Environment of a Site-Bound Metal Ion in the Hammerhead Ribozyme Determined by ^{15}N and ^{2}H ESEEM Spectroscopy. *J. Am. Chem. Soc.* **2006**, *128* (51), 16764–16770. https://doi.org/10.1021/ja057035p.

[39] Hunsicker-Wang, L.; Vogt, M.; DeRose, V. J. Chapter 16 - EPR Methods to Study Specific Metal-Ion Binding Sites in RNA. In *Methods in Enzymology*; Academic Press, 2009; Vol. 468, pp 335–367. https://doi.org/10.1016/S0076-6879(09)68016-2.

[40] Stich, T. A.; Lahiri, S.; Yeagle, G.; Dicus, M.; Brynda, M.; Gunn, A.; Aznar, C.; Derose, V. J.; Britt, R. D. Multifrequency Pulsed EPR Studies of Biologically Relevant Manganese(II) Complexes. *Appl Magn Reson* **2007**, *31*, 321–341. https://doi.org/10.1007/BF03166263.

[41] Hoogstraten, C. G.; Grant, C. V.; Horton, T. E.; DeRose, V. J.; Britt, R. D. Structural Analysis of Metal Ion Ligation to Nucleotides and Nucleic Acids Using Pulsed EPR Spectroscopy. *J. Am. Chem. Soc.* **2002**, *124* (5), 834–842. https://doi.org/10.1021/ja0112238.

[42] Tipton, P. A.; McCracken, J.; Cornelius, J. B.; Peisach, J. Electron Spin Echo Envelope Modulation Studies of Pyruvate Kinase Active-Site Complexes. *Biochemistry* **1989**, *28* (14), 5720–5728.

[42] Scott, R. A. In *Physical Methods in Bioinorganic Chemistry. Spectroscopy and Magnetism*; University Science Books: Sausalito, 2000, pp 465-503.

[43] Wu, P.; Yu, Y.; McGhee, C. E.; Tan, L. H.; Lu, Y. Applications of Synchrotron-Based Spectroscopic Techniques in Studying Nucleic Acids and Nucleic Acid-Functionalized Nanomaterials. *Advanced Materials* **2014**, *26* (46), 7849–7872. https://doi.org/10.1002/adma.201304891.

[44] Koutmou, K. S.; Casiano-Negroni, A.; Getz, M. M.; Pazicni, S.; Andrews, A. J.; Penner-Hahn, J. E.; Al-Hashimi, H. M.; Fierke, C. A. NMR and XAS Reveal an Inner-Sphere Metal

Binding Site in the P4 Helix of the Metallo-Ribozyme Ribonuclease P. *Proc. Nat. Acad. Sci USA* **2010**, *107* (6), 2479. https://doi.org/10.1073/pnas.0906319107.

[45] Sigel, H. Isomeric Equilibria in Complexes of Adenosine 5′-Triphosphate with Divalent Metal Ions. *European Journal of Biochemistry* **1987**, *165* (1), 65–72. https://doi.org/10.1111/j.1432-1033.1987.tb11194.x.

[46] Sternlicht, H.; Jones, D. E.; Kustin, K. Metal Ion Binding to Adenosine Triphosphate. III. Kinetic Analysis. *J. Am. Chem. Soc.* **1968**, *90* (25), 7110–7118. https://doi.org/10.1021/ja01027a041.

[47] Wee, V.; Feldman, I.; Rose, P.; Gross, S. Manganous-Adenosine Triphosphate System. Reinvestigation of Its Proton Magnetic Resonance Spectra. *J. Am. Chem. Soc.* **1974**, *96* (1), 103–112. https://doi.org/10.1021/ja00808a017.

[48] Potapov, A.; Goldfarb, D. Quantitative Characterization of the Mn^{2+} Complexes of ADP and ATPγS by W-Band ENDOR. *Applied Magnetic Resonance* **2006**, *30* (3), 461. https://doi.org/10.1007/BF03166212.

[49] Hunsicker, L. M.; DeRose, V. J. Activities and Relative Affinities of Divalent Metals in Unmodified and Phosphorothioate-Substituted Hammerhead Ribozymes. *Journal of Inorganic Biochemistry* **2000**, *80* (3), 271–281. https://doi.org/10.1016/S0162-0134(00)00079-9.

[51] Frey, P. A.; Sammons, R. D. Bond Order and Charge Localization in Nucleoside Phosphorothioates. *Science* **1985**, *228* (4699), 541–545.

[52] Liang, C.; Allen, L. C. Sulfur Does Not Form Double Bonds in Phosphorothioate Anions. *J. Am. Chem. Soc.* **1987**, *109* (21), 6449–6453. https://doi.org/10.1021/ja00255a034.

[53] Räsänen, J. P.; Peräkylä, M.; Pohjala, E.; Pakkanen, T. A. Ab Initio Studies on Organophosphorus Compounds. Part 2. Monoanionic Methyl Methylphosphonate and Methyl Methylphosphinate and Their Sulfur Analogues. *J. Chem. Soc., Perkin Trans. 2* **1994**, No. 5, 1055–1060. https://doi.org/10.1039/P29940001055.

[54] Pichierri, F.; Sarai, A. Properties of Phosphorothioate DNA Analogs. An Ab Initio Study of Prototype Model Linkages Derived from Dimethyl-Phosphate Anion. *Journal of Molecular Structure: THEOCHEM* **1999**, *460* (1), 103–116. https://doi.org/10.1016/S0166-1280(98)00309-1.

[55] Pearson, R. G. Absolute Electronegativity and Hardness: Application to Inorganic Chemistry. *Inorg. Chem.* **1988**, *27* (4), 734–740. https://doi.org/10.1021/ic00277a030.

[56] Dahm, S. C.; Uhlenbeck, O. C. Role of Divalent Metal Ions in the Hammerhead RNA Cleavage Reaction. *Biochemistry* **1991**, *30* (39), 9464–9469. https://doi.org/10.1021/bi00103a011.

[57] Basu, S.; Strobel, S. A. Thiophilic Metal Ion Rescue of Phosphorothioate Interference within the Tetrahymena Ribozyme P4-P6 Domain. *RNA* **1999**, *5* (11), 1399–1407.

[58] Yean, S.-L.; Wuenschell, G.; Termini, J.; Lin, R.-J. Metal-Ion Coordination by U6 Small Nuclear RNA Contributes to Catalysis in the Spliceosome. *Nature* **2000**, *408* (6814), 881–884. https://doi.org/10.1038/35048617.

[59] Coggins, M. K.; Toledo, S.; Shaffer, E.; Kaminsky, W.; Shearer, J.; Kovacs, J. A. Characterization and Dioxygen Reactivity of a New Series of Coordinatively Unsaturated Thiolate-Ligated Manganese(II) Complexes. *Inorg. Chem.* **2012**, *51* (12), 6633–6644. https://doi.org/10.1021/ic300192q.

[60] Brines, L. M.; Shearer, J.; Fender, J. K.; Schweitzer, D.; Shoner, S. C.; Barnhart, D.; Kaminsky, W.; Lovell, S.; Kovacs, J. A. Periodic Trends within a Series of Five-Coordinate Thiolate-Ligated $[M^{II}(SMe_2N_4(Tren))]^+$ (M = Mn, Fe, Co, Ni, Cu, Zn) Complexes, Including a Rare Example of a Stable Cu^{II}–Thiolate. *Inorg. Chem.* **2007**, *46* (22), 9267–9277. https://doi.org/10.1021/ic701433p.

[61] Hunsicker, L. M.; DeRose, V. J. Activities and Relative Affinities of Divalent Metals in Unmodified and Phosphorothioate-Substituted Hammerhead Ribozymes. *Journal of Inorganic Biochemistry* **2000**, *80* (3), 271–281. https://doi.org/10.1016/S0162-0134(00)00079-9.

[62] Shan, S.-O.; Herschlag, D. An Unconventional Origin of Metal-Ion Rescue and Inhibition in the Tetrahymena Group I Ribozyme Reaction. *RNA* **2000**, *6* (6), 795–813. https://doi.org/10.1017/S1355838200000649.

[63] Cunningham, L. A.; Li, J.; Lu, Y. Spectroscopic Evidence for Inner-Sphere Coordination of Metal Ions to the Active Site of a Hammerhead Ribozyme. *J. Am. Chem. Soc.* **1998**, *120* (18), 4518–4519. https://doi.org/10.1021/ja973251p.

[64] Osborne, E. M.; Ward, W. L.; Ruehle, M. Z.; DeRose, V. J. The Identity of the Nucleophile Substitution May Influence Metal Interactions with the Cleavage Site of the Minimal Hammerhead Ribozyme. *Biochemistry* **2009**, *48* (44), 10654–10664. https://doi.org/10.1021/bi900614v.

[65] Slim, G.; Gait, M. J. Configurationally Defined Phosphorothioate-Containing Oligoribonucleotides in the Study of the Mechanism of Cleavage of Hammerhead Ribozymes. *Nucleic Acids Research* **1991**, *19* (6), 1183–1188. https://doi.org/10.1093/nar/19.6.1183.

[66] de Meester, P.; Goodgame, D. M. L.; Jones, T. J.; Skapski, A. C. X-Ray Evidence for Metal–N-7 Bonding in a Hydrated Manganese Derivative of Guanosine 5′-Monophosphate. *Biochemical Journal* **1974**, *139* (3), 791–792. https://doi.org/10.1042/bj1390791.

[67] Sturgeon, B. E.; Britt, R. D. Sensitive Pulsed EPR Spectrometer with an 8–18 GHz Frequency Range. *Review of Scientific Instruments* **1992**, *63* (4), 2187–2192. https://doi.org/10.1063/1.1143136.

[68] Sturgeon, B. E.; Ball, J. A.; Randall, D. W.; Britt, R. D. ^{55}Mn Electron Spin Echo ENDOR of Mn^{2+} Complexes. *J. Phys. Chem.* **1994**, *98* (49), 12871–12883. https://doi.org/10.1021/j100100a012.

[69] Zabinsky, S. I.; Rehr, J. J.; Ankudinov, A.; Albers, R. C.; Eller, M. J. Multiple-Scattering Calculations of x-Ray-Absorption Spectra. *Phys. Rev. B* **1995**, *52* (4), 2995–3009. https://doi.org/10.1103/PhysRevB.52.2995.

[70] Frisch M, Schlegel H, Scuseria G et al (2016) Gaussian09. Gaussian Inc., Wallingford

Sample	Fit	Shell	R_{as}(Å)	σ_{as} (Å)^2	ΔE_o	f
Mn-WT	1	Mn-O6	2.18	0.0054	-1.30	0.085
	2	Mn-O6 Mn-(C,N,O)3	2.18 3.08	0.0053 0.0118	-1.73	0.076
	3	Mn-O6 Mn-(S,P)	2.18 3.41	0.0054 0.0167	-1.47	0.083
	4	Mn-O6 Mn-(C,N,O)3 Mn-(S,P)	2.18 3.06 3.49	0.0053 0.0094 0.0096	-1.80	0.074
Mn-A9-S_{Sp}	5	Mn-O6	2.21	0.0076	-1.09	0.095
	6	Mn-O6 Mn-(C,N,O)3	2.21 3.06	0.0074 0.0052	-1.62	0.076
	7	Mn-O6 Mn-(S,P)	2.21 3.33	0.0076 0.0079	-1.71	0.090
	8	Mn-O6 Mn-(C,N,O)3 Mn-(S,P)	2.21 3.05 3.43	0.0074 0.0050 0.0127	-1.80	0.074
Mn-A9-S_{Rp}	9	Mn-O6	2.21	0.0070	-1.59	0.096
	10	Mn-O6 Mn-(C,N,O)3	2.20 3.04	0.0069 0.0054	-2.24	0.077
	11	Mn-O6 Mn-(S,P)2	2.20 3.32	0.0069 0.0108	-2.48	0.086
	12	Mn-O6 Mn-(C,N,O)3 Mn-(S,P)2	2.20 3.01 3.36	0.0067 0.0024 0.0024	-2.88	0.069
Mn-ATP	13	Mn-O6 Mn-P6	2.15 3.34	0.0055 0.0108	-3.45	0.100
	14	Mn-O6 Mn-P3	2.15 3.35	0.0054 0.0041	-2.72	0.096
	15	Mn-O6 Mn-P2	2.15 3.35	0.0053 0.0012	-2.45	0.096

Table 1. Curve-fitting results for Mn EXAFS data on tHHRz and Mn-ATP model compound. Shell defines a set of like atoms at the same distance. N_s is the number of scatterers per metal. R_{as} is the metal-scatterer distance. σ_{as}^2 is the mean square deviation in R_{as}. ΔE_o is the shift in E_o for the theoretical scattering functions, and f is a normalized chi-squared error.

Sample	Shell	R_{as}(Å)	σ_{as} (Å)^2	ΔE_o	f
Mn EXAFS					
Mn-GMP	Mn-O5 Mn-N	2.19 2.09	0.0032 0.0001	2.07	0.064
Mn-ATPγS	Mn-O6 Mn-(C,N,O)3 Mn-(S,P)	2.16 3.11 3.32	0.0050 0.0056 0.0020	2.12	0.110
Mn-A9-S_{Rp} (in $(NO_3)^-$)	Mn-O6 Mn-(S,P)	2.17 3.37	0.0021 -.0010	2.42	0.129
Cd EXAFS					
Cd-WT	Cd-O6	2.40	0.0032	1.80	0.112
Cd-A9-S_{Sp}	Cd-O6	2.41	0.0022	4.23	0.113
	Cd-O5 Cd-S1	2.36 2.59	0.0033 -0.0011	-1.54	0.118
Cd-A9-S_{Rp}	Cd-O6	2.42	0.0018	3.21	0.136
	Cd-O5 Cd-S1	2.37 2.60	0.0028 -0.0007	-3.58	0.087

Table 2. Curve-fitting results for EXAFS data obtained on Mn-model compounds, Mn-tHHRz A9-S_{Rp} with NO_3^- counterions, and on Cd-substituted tHHRz samples. Shell defines a set of like atoms at the same distance. N_s is the number of scatterers per metal. R_{as} is the metal-scatterer distance. σ_{as}^2 is the mean square deviation in R_{as}. ΔE_o is the shift in E_o for the theoretical scattering functions, and f is a normalized chi-squared error.

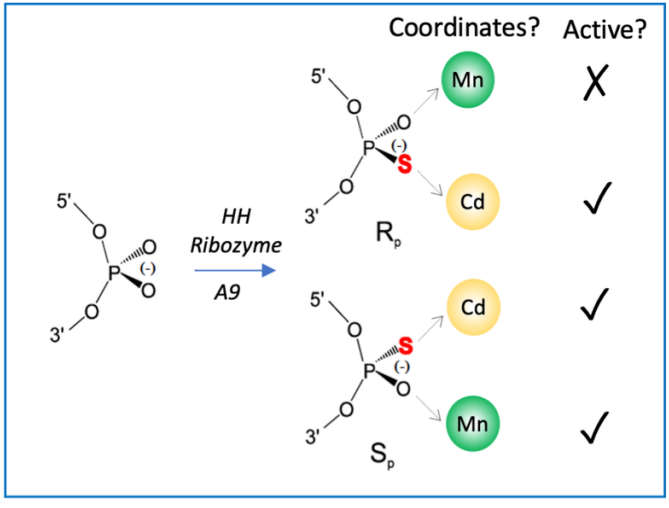

Synopsis: Mn and Cd coordination to phosphorothioates in a ribozyme metal site determined by EPR and EXAFS spectroscopies